December, 2012 Vol.12, No.4

Journal of Pipeline Engineering

incorporating

The Journal of Pipeline Integrity

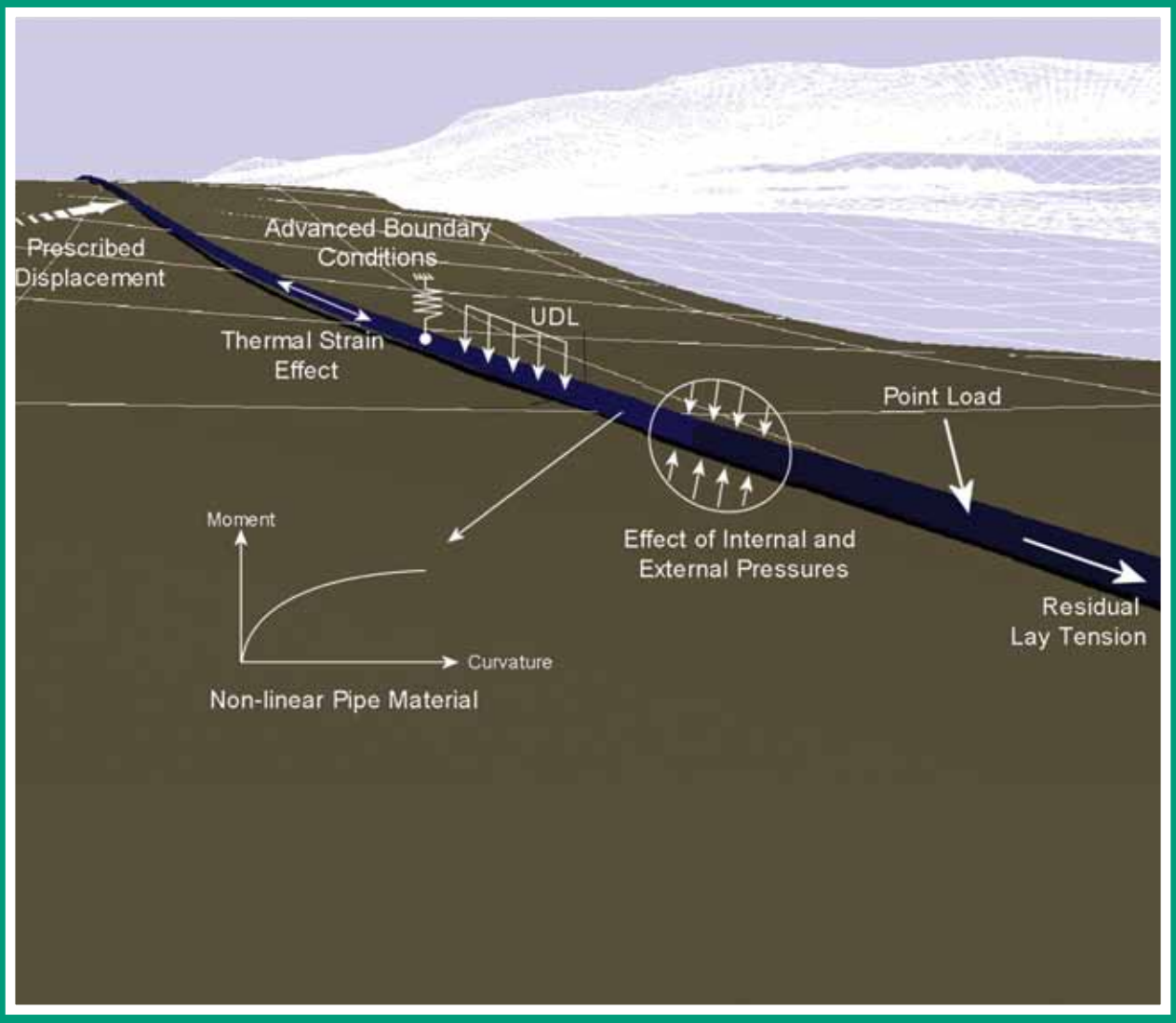

Great Southern Press

Clarion Technical Publishers

Journal of Pipeline Engineering

Editorial Board - 2012

The Journal of Pipeline Engineering

incorporating

The Journal of Pipeline Integrity

Volume 12, No 4 • Fourth Quarter, 2012

Contents

❖ ❖ ❖

OUR COVER PICTURE shows a graphic of typical loading pattern for a subsea pipeline. The figure is taken from the paper on pages 273-286 which examines the issue of numerical modelling and analysis for the design, installation, and operation of subsea pipelines.

The Journal of Pipeline Engineering has been accepted by the Scopus Content Selection & Advisory Board (CSAB) to be part of the SciVerse Scopus database and index.

Numerical modelling and analysis for offshore pipeline design, installation, and operation

by Dr Filip Van den Abeele* and Raphael Denis
Fugro GeoConsulting Belgium, Brussels, Belgium

THE INCREASING demand for oil and gas, currently estimated at 135 million barrels of oil equivalent per day, keeps pushing the boundaries of offshore engineering into ever-deeper waters. For instance, in the Gulf of Mexico, exploration and production activities are performed in water depths exceeding 3000 m. Such remote locations and challenging environments call for new procedures and solutions in the design and installation of offshore pipelines.

In this paper, numerical modelling and analysis of offshore pipelines is reviewed and discussed. Finite-element techniques to assist in pipeline design are introduced, and applied to pipeline routeing optimization. Special emphasis is devoted to out-of-straightness and on-bottom stress analysis.

Contact algorithms allowing the simulation of pipelaying on an uneven seabed (using bathymetry) are reviewed, and recent developments in modelling of pipe-soil interaction are highlighted. The importance of free-span detection and evaluation is stressed. In addition, it is shown how finite-element analysis can contribute to the prediction and mitigation of both upheaval and lateral buckling of subsea pipes. At the end of this paper, pipeline walking on an inclined seabed is simulated, and the importance of seabed friction on the walking rate is demonstrated.

OIL AND GAS exploration and production is embarking into ever greater water depths. Consequently, offshore pipeline engineering is continuously pushing the boundaries, installing flowlines and export pipelines in water depths exceeding 3000 m. The availability of high-performance computing systems and dedicated software tools enable pipeline engineers to cope with the challenges associated with design of subsea completions.

In this paper, an overview is presented of numerical modelling and analysis for offshore pipeline design, installation, and operation. *SAGE Profile 3D* [1-3] is used to demonstrate the added value of numerical modelling as a design aid and decision tool throughout the entire life of an offshore pipeline, covering:

- preliminary pipeline design
- route selection and optimization
- offshore pipeline installation
- free-span assessment
- on-bottom stress analysis

*Corresponding author's contact details
tel: +32 497 548 916
email: filip@vikar.be

SAGE Profile 3D uses a transient dynamic explicit integration kernel, which enables the efficient simulation of the pipelaying process and the response of the subsea pipe when subjected to hydrodynamic loading and operational conditions (time-dependent pressure and temperature profiles). In this paper, the numerical algorithms governing pipeline laydown, pipe-soil interaction, and numerical integration are briefly covered, and some examples on free-span evaluation, lateral buckling, upheaval buckling, and pipeline walking are highlighted to demonstrate the versatility of finite-element methods as a powerful support tool in offshore pipeline design.

Pipeline route selection and optimization

One of the early tasks for the pipeline engineer is to determine the preliminary route and evaluate the feasibility of the selected pipeline corridor. An informed route selection cannot be made without information on the seabed topography and geotechnical data [4].

Performing an initial desk study before embarking on an extensive (and expensive) marine survey can save a considerable amount of time and money [5]. In *SAGE Profile*,

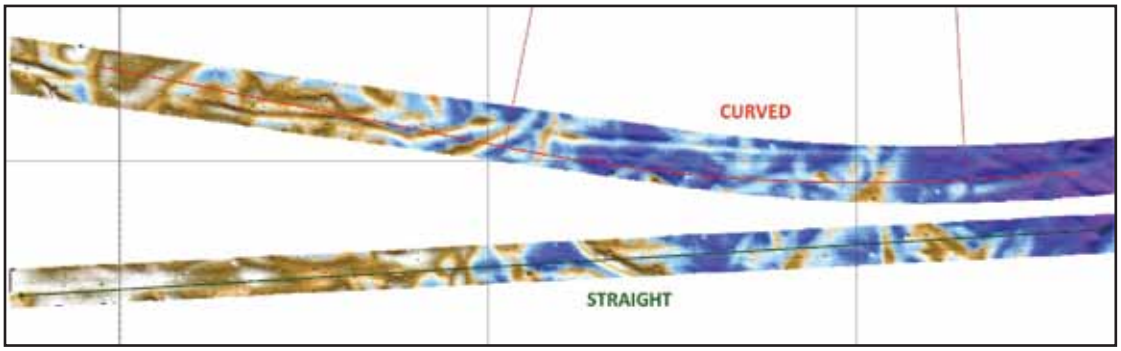

Fig.1. 3D digital-terrain model based on survey data.

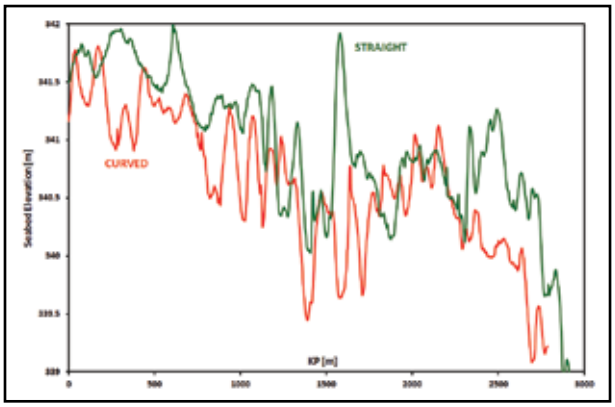

Fig.2. Early assessment of seabed topography.

the seabed topology can easily be created or imported from survey data, either as:

- kilometre point (KP) versus seabed elevation
- Easting-Northing-elevation (ENE) coordinates
- full 3D digital-terrain model (DTM)

In Fig.1, two corridors imported from survey data are compared. In the northern corridor, a curved pipeline route has been drawn, whilst a straight pipeline section is proposed for the southern part.

The pipeline route can be easily imported, or constructed through a user-friendly and straightforward graphical interface. This interface will convert the constructed route automatically into a proprietary route format, with successive sections of straight lines and circle arcs. The straight sections (like the green route in Fig.1) are defined by a start and end point, whereas the circular arcs (for example, the middle section of the red route shown in Fig.1) are defined by the tangent points and the centre of the circle linking these tangent points.

As demonstrated in Fig.2, the user interface enables an early assessment of seabed topography and on-bottom roughness. Whilst modifying the proposed pipeline route, the graph of seabed elevation versus KP is updated simultaneously, which allows evaluating the on-bottom roughness of the selected route already during pre-processing, without any requirement for computing power.

At the same time, the allowable bending radii can be quickly screened. Each pipeline bend radius R should be large enough to ensure that the bending stresses do not exceed the allowable stress σ_a:

$$R > \frac{E\, D_o}{2\, \sigma_a} \tag{1}$$

where E is the Young's modulus of the pipeline steel and Do is the outer diameter of the pipe. Moreover, the pipeline requires sufficient frictional force to resist being dragged over the seabed by the lay barge. Hence:

$$R > \frac{T}{\mu\, w_s} \tag{2}$$

with μ the lateral friction factor, T the lay tension, and w_s the submerged weight per unit length. In addition to bathymetric considerations, selection of the optimum pipeline route also depends on a broad spectrum of other factors, including:

- politics and regulatory requirements
- crossing of existing pipelines or submarine cables
- iceberg plough marks, pockmarks
- areas of very soft or very hard seabed
- boulder fields, rock outcrops
- risk of anchor damage and trawling gear impact
- proximity of other subsea installations
- cost-efficiency of installation
- environmental and ecological issues
-

The *SAGE Profile* pre-processor allows introduction of different layers of information, by importing additional information such as admiralty charts, test locations, existing pipelines, and shipwrecks. In Fig.3, for instance, a proposed pipeline route is shown on a digital-terrain model and, in addition, an overlay plot is made to display data associated

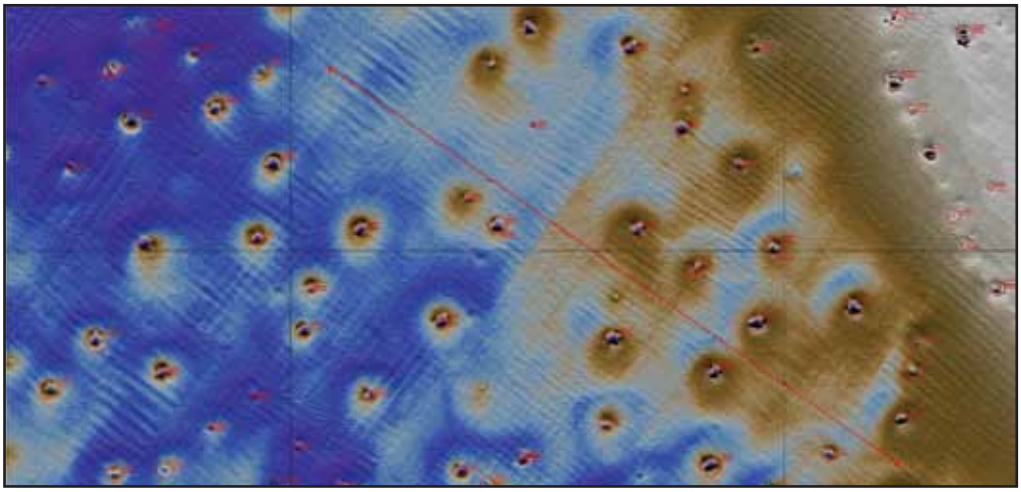

Fig.3. Digital-terrain model with pockmark indications.

with the pockmarks. This layered presentation of information offers the pipeline designer an intuitive dashboard with a wealth of data to select the most appropriate pipeline route. In addition to overlay plots, contour maps, and slope angles can easily be visualized, which provides additional input to assess potential geohazards.

Simulating pipe laydown and installation

Offshore pipeline installation is performed from a laybarge, typically in S-lay configuration. For smaller diameters, pipeline reeling can be the most cost efficient solution, whereas J-lay is the only feasible approach in (ultra-) deep water. Depending on the installation method, the pipeline is subjected to different load patterns during installation, including hydrostatic pressure, lay tension, and bending on the stinger and in the sagbend. A comprehensive overview on the mechanics of installation design can be found in [6].

The simulation of the pipelaying process is one of the most challenging tasks once the optimum route has been selected. Implementing pipeline installation in a general-purpose finite-element package can be a time-consuming and tedious job, in particular when importing vast amounts of seabed data. Most often, advanced scripting techniques are required to define the seabed profile, select the optimum pipeline route, and simulate the laydown process. In addition, the available constitutive models for pipe-soil interaction may not comply with industry standards.

Finite element tools like *SAGE Profile* have been tailored to assist the pipeline engineer during offshore pipeline design. Using an explicit integration algorithm, the actual pipeline-installation process can be approximated. The pipe is simulated by discretising the entire pipeline into section of finite length. These sections are represented by beam elements with 12 degrees of freedom (DOF), bounded at either side by nodes. The distributed mass of the pipe is lumped at these nodes. The finite-element kernel uses an explicit solver, which computes the dynamic motion of the pipe and is therefore ideally suited to simulate the pipelaying process.

During this pipeline installation process, new pipe elements are continuously created and the pipe is laid along the target path defined on the seabed. The lay tension T, applied at the barge, is used as an input and the unstressed length L_0 of the last element is updated such that the axial force corresponds to the applied lay tension:

$$\frac{L - L_0}{L_0} EA - F_p = T \tag{3}$$

with L the original element length,

$$A = \frac{\pi}{4} (D_o^2 - D_i^2) \tag{4}$$

the cross-sectional area of a circular pipe with inner diameter D_i and outer diameter D_o, and

$$F_p = (1 - 2\nu)(p_o A_o - p_i A_i) \tag{5}$$

the pressure induced axial force component, accounting for both the internal pressure p_i and the (hydrostatic) external pressure p_o. As a result, both empty and water-filled installation can be simulated. In Equn 3, ν is the Poisson's coefficient of the pipeline steel, where A_i and A_o are the surface areas of the interior and exterior of the pipe respectively. When the unstressed element length:

$$L_0 = \frac{L\ E\ A}{T + F_p + E\ A} \tag{6}$$

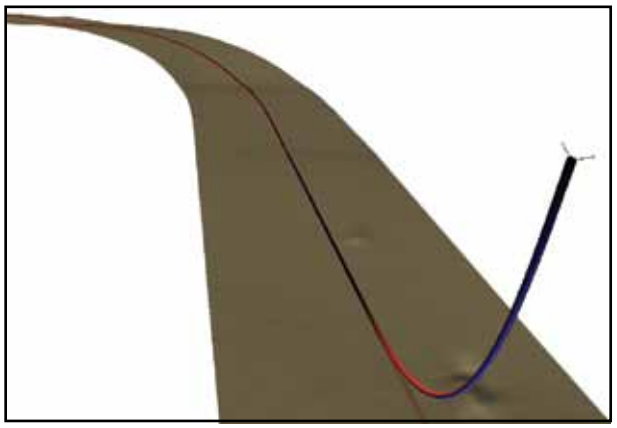

Fig.4. Pipeline catenary shape during S-lay installation.

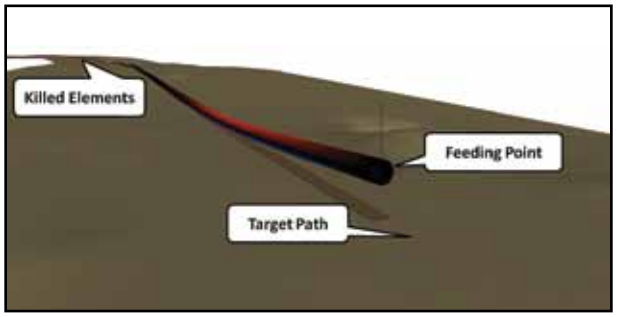

Fig.5. Definition of feeding point and target path.

becomes longer than twice the initial length, the element is split in two new elements. An additional node is placed along the last element such that the newly formed element obtains the original unstressed length. This algorithm accurately reflects the continuous supply of welded pipe joints from a moving laybarge. Gravity, applied during the pipelay simulation, will force the newly created pipe elements into place; Fig.4 shows the typical catenary shape during pipeline installation.

For long pipelines and significant water depths, simulating the entire laydown process (from the barge down to the seabed) tends to be time-consuming and is computationally expensive. The sophisticated architecture of the currently available numerical solvers allows for a significant reduction in the resources required to simulate pipeline laydown. By default, the laybarge and most of the free-hanging pipe is replaced by a single feeding point in the water column moving close to the seabed, as shown in Fig.5. This feeding point acts as a submarine laybarge, generating new pipe joints as it moves forward. The lay tension is now applied at the feeding point, generating a residual on-bottom tension in the laid pipe section.

Assuming a catenary shape [6], the lay tension at the feeding point can be expressed in terms of the submerged weight per unit length w_s:

$$T = \frac{h\, w_s}{\tan^2 \theta} \left(1 + \sqrt{1 + \tan^2 \theta}\right) \quad (7)$$

where θ is the angle between the pipe and the target path, and h is the height of the feeding point above the seabed. Replacing the laybarge with a feeding point close to the seabed allows for a significant reduction in calculation time, without losing accuracy. Given the inherent complexity of pipeline laying, an accurate and robust steering mechanism of the feeding point is of paramount importance. In *SAGE Profile*, this steering mechanism is governed by a proportional-integrating-differentiating (PID) controller, providing a smooth movement of the feeding point and ensuring that the pipeline is installed on the pre-defined target path (shown in red in Fig.5).

In addition to the concept of a feeding point, an efficient element-killing procedure has been implemented to control the computational effort during pipeline laydown. Indeed, it would be too expensive to simulate the entire length of the pipe from its starting point up to the feeding point. In order to reduce the required calculation time, elements that are already lying on the seabed and are no longer moving will be removed from the simulation. If the magnitude of the velocity vector for a node is lower than a predefined threshold, the associated element has little or no contribution to the simulation results and can be killed without losing accuracy. In Fig.5, the elements that have been killed are also shown.

Evaluation of free-spanning pipelines

Accurate prediction of free spans (location, length, and height) is an important prerequisite in offshore pipeline design. Indeed, free-span lengths should be maintained within an allowable range [7], which is determined during the design phase. Pipelines installed on a very rough seabed can cause a high number of free spans that can be difficult to rectify. A judicious assessment of free spans can dramatically reduce the costs associated with seabed intervention (trenching, rock dumping, and span supports).

Figure 6 demonstrates that finite-element analyses enable the simulation of pipeline installation on an uneven seabed, and allow detection of free spans. The colour code on Fig.6 reflects the local span height, i.e. the gap between the pipeline and the seabed. After the pipelay simulation has been completed, *SAGE Profile* automatically detects the spans over the entire pipeline route, and plots the span location, length and height in comprehensive and easy-to-read design charts, as shown in Fig.7.

Once a free span that is longer than the allowable span length occurs, the span may suffer from vortex-induced vibrations (VIV) which can induce fatigue damage in the pipe. It was only recently that the commonly used pipeline design codes allow free vibrating spans, as long as the structural integrity of the pipeline system remains assured [8].

Span checks can be performed to assess whether an installed pipe is compliant with the guidelines recommended in

DNV-RP-F105 [9]. For each detected span, *SAGE Profile* will calculate the associated reduced velocity:

$$V_R = \frac{U_c + U_w}{f_1 D_o} \tag{8}$$

where U_c is the mean current velocity (normal to the pipe), U_w the significant wave-induced flow velocity, and f_1 an approximation [9] for the lowest natural frequency given by:

$$f_1 \approx \sqrt{1 + CSF} \sqrt{\frac{EI}{m_e L_e^4}\left[1 + \frac{F_e}{P_{cr}} + C_3\left(\frac{\delta}{D_o}\right)^2\right]} \tag{9}$$

with SCF the stiffening effect of the concrete coating, L_e the effective span length [10], m_e the effective mass, F_e the effective axial force, δ the static deflection and C_3 the end boundary coefficient. The moment of inertia for the hollow circular pipe is given by

$$I = \frac{\pi}{64}\left(D_o^2 - D_i^2\right) \tag{10}$$

and the critical buckling load can be calculated as

$$P_{cr} = (1 + SCF)\, C_2 \left(\frac{\pi}{L_e}\right)^2 EI \tag{11}$$

where C_2 is an end boundary coefficient as well.

In addition to the reduced velocity (Equn 8), the software calculates the stability parameter:

$$K_s = 4\pi \frac{m_e \zeta_T}{\rho_w D_o^2} \tag{12}$$

for each span, where ζ_T is the total modal damping ratio, comprising structural damping, hydrodynamic damping and soil damping. Based on the values of the reduced velocity from Equn 8 and the corresponding stability parameter from Equn 12, the software will check whether the conditions for the onset of in-line or cross-flow VIV are met in full compliance with DNV-RP-F105. This powerful capability provides a quick and easy tool to evaluate the severity of free spans for a given pipeline route, and hence can save a tremendous amount of time and money associated with seabed rectification.

In the next sections, some operational analyses are presented to evaluate the susceptibility of high-temperature subsea pipelines for buckling and walking. First, some details and recent developments on numerical modelling of pipe-soil interaction are reviewed.

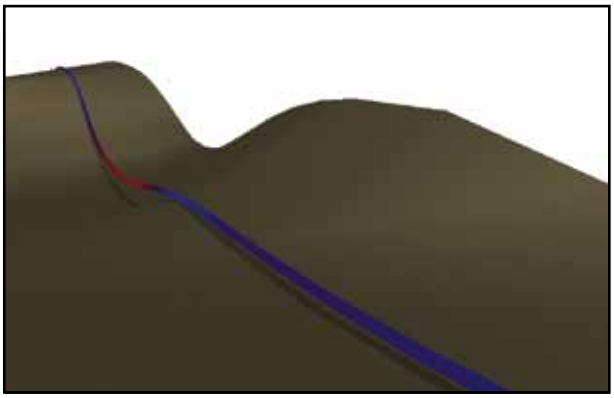

Fig.6. Free-spanning pipeline on an uneven seabed.

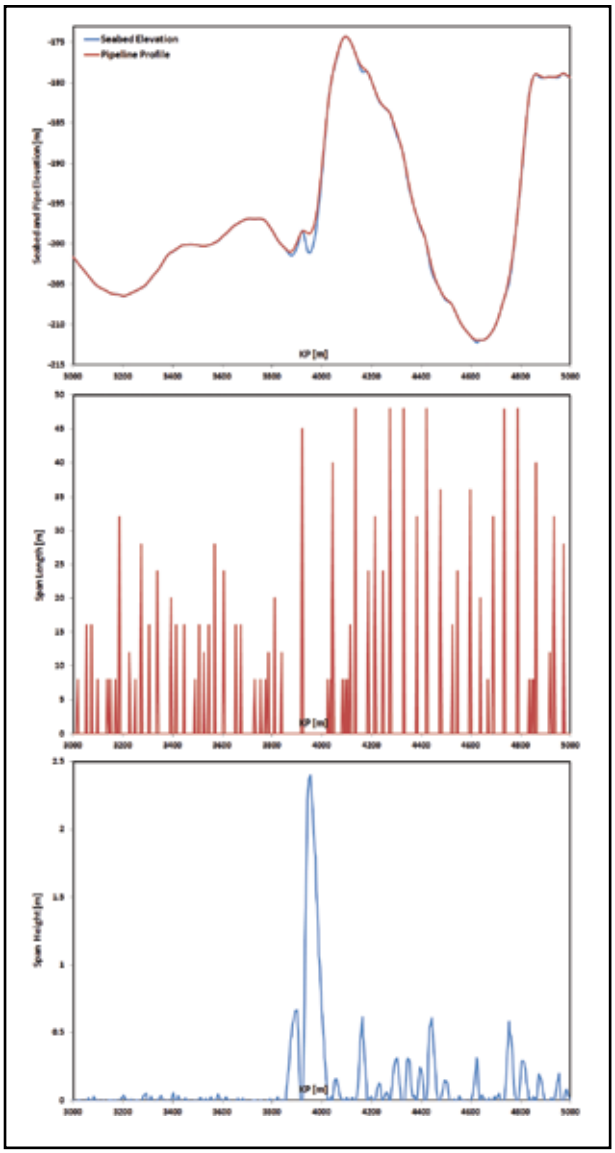

Fig.7. Overview of span location, height, and length.

Numerical modelling of pipe-soil interaction

The key to a successful simulation of offshore pipeline installation and operation is a profound understanding of the pipe-soil interaction, which is the most important parameter governing the design. The elastoplastic constitutive behaviour of the pipeline steel can be described by the Ramberg-Osgood equation [11-12], connecting pipe

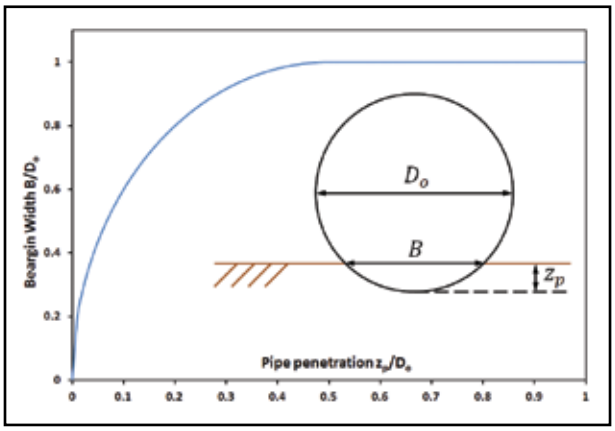

Fig.8. Bearing width as a function of pipe penetration.

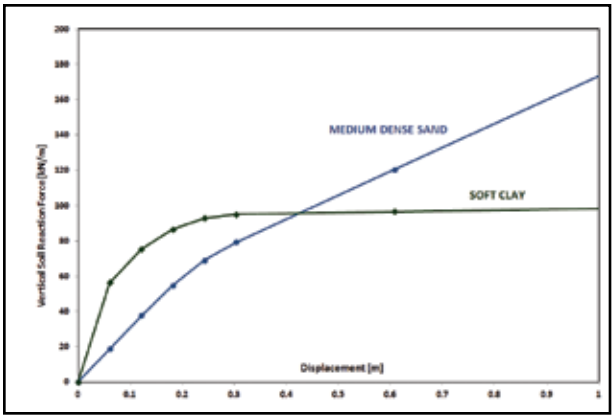

Fig.9. Vertical soil reaction for sand and clay.

curvature κ with bending moment M through:

$$\frac{\kappa}{\kappa_0} = \frac{M}{M_0} + \alpha \left(\frac{M}{M_0}\right)^{\beta} \tag{13}$$

where the nominal curvature κ_0 and bending moment M_0 are related by:

$$\frac{M_0}{\kappa_0} = EI \tag{14}$$

and the parameters α and β are chosen to fit the moment-curvature relationship obtained by integrating the stresses across the section A for a given curvature:

$$M = \int_A \sigma_{xx}\, y\, dA \tag{15a}$$

Hence, Equn 13 is equivalent to the well-known stress/strain relationship [11, 13]:

$$\varepsilon(\sigma) = \frac{\sigma}{E} + K \left(\frac{\sigma}{\sigma_y}\right)^n \tag{15b}$$

with σ_y the yield stress and {K,n} the parameters describing the hardening behaviour of the steel grade. The enhanced Ramberg-Osgood formulation in *SAGE Profile* takes into account the combined effects of plasticity, ovalization [14-15], axial force, and hydrostatic pressure ([15-16].

The pipe is assumed to be in contact with the seabed when the difference between the z-coordinate of a pipe node and the corresponding seabed elevation at this (x,y) location is less than the external pipe radius R_o. Once contact has been detected, a soil response will be exerted depending on the type of seabed soil. The soil response is captured by a combination of vertical, axial and lateral springs.

The bearing capacity Q_u is reflected by the vertical soil reaction. For sands, DNV-RP-F105 recommends:

$$Q_u(z_p) = \left(\frac{\gamma_s N_\gamma}{2} B(z_p) + \gamma_s z_p N_q\right) B(z_p) \tag{16}$$

where γ_s is the submerged unit weight,

$$N_q = \exp(\pi \tan\varphi)\, \tan^2\left(\frac{\pi}{4} + \frac{\varphi}{2}\right) \tag{17}$$

with φ the friction angle, and

$$N_\gamma = \frac{3}{2}\left(N_q - 1\right)\tan\varphi \tag{18}$$

The bearing width B depends on the pipe penetration z_p, as is schematically shown in Fig.8, and can be calculated as:

$$B(z_p) = \begin{cases} 2\sqrt{z_p(D_o - z_p)} & 0 \le z_p \le D_o/2 \\ D_o & \text{otherwise} \end{cases} \tag{19}$$

For clays, DNV-RP-F105 recommends:

$$Q_u(z_p) = \left(5.14\, C_u + \gamma_s\, z_p\right) B(z_p) \tag{20}$$

where C_u is the undrained shear strength. Figure 9 compares the vertical soil-spring reaction forces for a medium-dense sand (with a friction angle φ = 33° and a submerged unit weight γ_s= 8.5 kN/m³) with the soil reaction of a soft clay (with undrained shear strength C_u = 30 kPa and a submerged unit weight γ_s= 7.5 kN/m³).

In addition to the vertical soil springs recommended by DNV-RP-F105 [9], other soil models for both cohesive and cohesionless materials are described in DNV- CN30.4 [17-18]. For very soft clays (C_u < 20 kPa), a buoyancy formulation could be used, assuming that the soil behaves like a liquid and that the soil-induced buoyancy of the pipeline is equal to the vertical soil reaction:

$$Q_u(z_p) = \frac{z_p}{6\, B(z_p)}\left(3\, z_p^2 + 4B^2(z_p)\right)\gamma_s \tag{21}$$

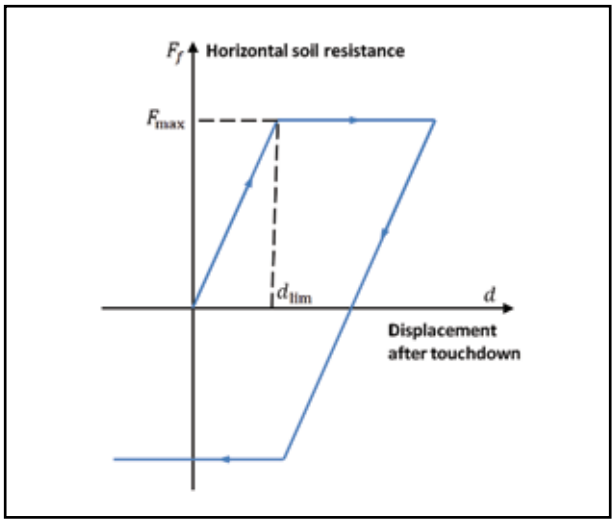

Fig. 10. Frictional spring with memory component.

For rock, either a rigid seabed or clay with a (very) high undrained shear strength, can be modelled. In addition to the vertical soil spring, reflecting the bearing capacity of the seabed, axial and lateral springs are included in the formulation of pipe soil interaction. As shown in Fig.10, such springs allow for energy dissipation through friction and have a memory component which is instrumental for simulating plastic soil deformation, for example the pipeline walking phenomenon discussed below. As soon as contact is made with the seabed, the coordinates of the first point of seabed touchdown are saved for each node. The distance the node subsequently travels while in contact with the seabed determines the amount of compression exerted on the lateral and axial soil springs.

The input values required to define the axial and lateral soil springs are:

- the threshold displacement d_{lim} after touchdown
- the adhesion F_{adh}
- the dimensionless friction factor μ

The distance d_f to the touchdown point in axial and lateral direction is computed, and converted into a friction force defined by the soil springs. If the displacement is smaller than the threshold, a friction force:

$$F_f = \frac{d_f}{d_t} F_{\max} \tag{22}$$

is applied, where the maximum friction force is given by:

$$F_{\max} = F_{adh} + \mu F_V \tag{23}$$

with F_V the vertical load per unit length. If the displacement is larger than the threshold, than the friction force is equal to F_{max}, i.e. the soil behaves as perfectly plastic. As indicated in Fig.10, the unloading path differs from the loading curve, which allows for frictional energy dissipation.

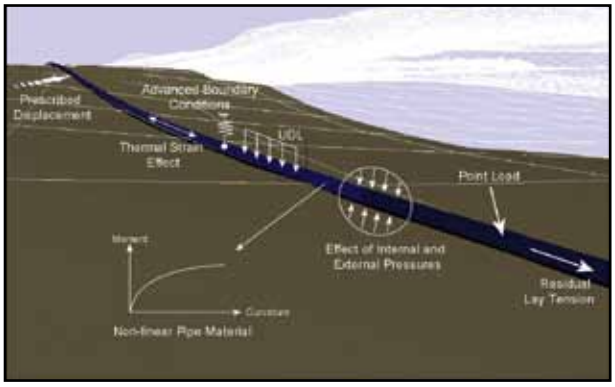

Fig. 11. Load patterns acting on a subsea pipeline.

The combination of a vertical, axial and lateral soil spring fully defines the pipe-soil interaction. In addition to the commonly used soil-spring models, presented here, *SAGE Profile* offers dedicated and more enhanced soil models to describe complex soil behaviour such as berm formation, buried pipes, and trenching operations [19]. Moreover, an application programming interface (API) can be used to access an advanced soil library based on the incremental plasticity approach described by Zhang [20-21]. In this approach, the load-displacement relationship for an elastoplastic soil model is expressed in its incremental form:

$$\{dU\} = [C]\{dF\} \tag{24}$$

where the vector of incremental loads $\{dF\}$ is connected to the resulting displacements $\{dU\}$ by the compliance matrix [C]. In addition to an extensive library of predefined soil models, user-defined constitutive laws can be implemented as well to construct the compliance matrix.

Accurate pipe-soil interaction is a key requirement for the reliable prediction of the on-bottom behaviour of offshore pipelines. Significant development efforts are being conducted to continuously improve the predictive capability of the pipe-soil interaction parameters [22]. Recently, much R&D effort has been devoted to the development of coupled soil springs to comply with the guidelines of the SAFEBUCK JIP [23-24].

In the next sections, some case studies on pipeline instability (lateral buckling, upheaval buckling, and pipeline walking) are presented to demonstrate the importance of pipe-soil interaction in finite-element simulations. First, the numerical architecture of the transient dynamic solver is briefly explained.

Loading patterns and explicit integration

Offshore pipelines are subjected to hydrodynamic loading (combined actions of currents and waves), internal and external pressure, operational loads (temperature and pressure), and external loads. As is schematically shown in Fig.11, these loads can be either defined directly (for example, lay tension,

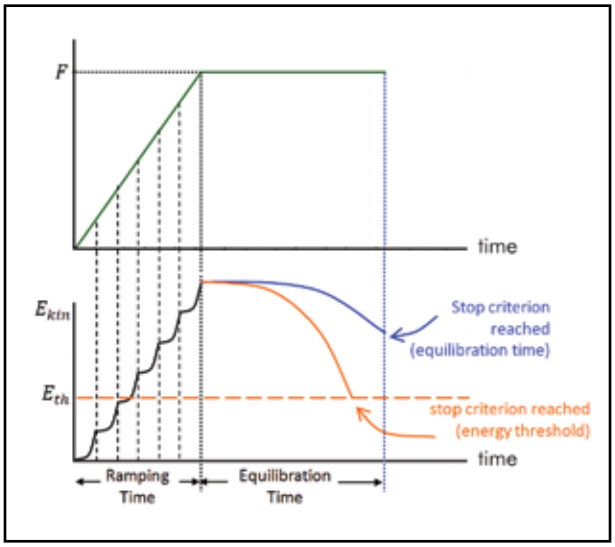

Fig. 12. Introduction of quasi-static loading.

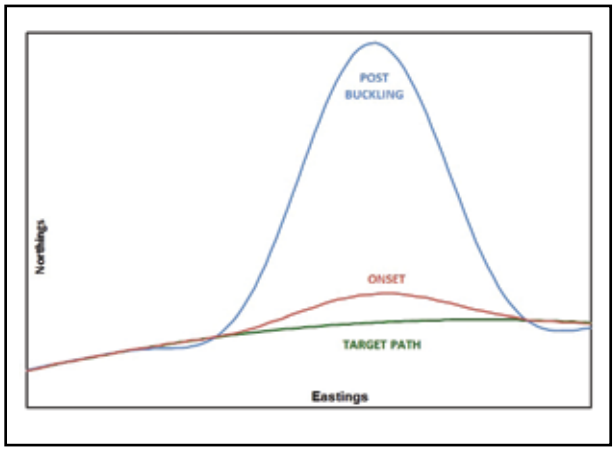

Fig. 13. SAGE Profile simulation of lateral buckling.

operational pressure and temperature) or modelled using either uniformly distributed loads (such as to model buried pipe sections), point loads (such as to reflect the additional mass of sacrificial anodes), or pre-described displacements (such as the pipeline being lifted by the plough grabs during trenching operations).

Internal and external pipe pressure are modelled by taking into account the water depth at each node. Temperature profiles can vary with KP, reflecting the temperature gradient between the hot end (close to the wellhead or manifold) and the cold end (riser tie-in). Pressure and temperature variations (as well as the residual bottom tension after lay-down) contribute to the nodal forces. Assuming that waves are approaching the pipeline with a velocity u and at an angle α, and the current with steady velocity V is approaching at an angle β, both a lift force:

$$F_L = \frac{1}{2} C_L \rho_w D_o (u\cos\alpha + V\cos\beta)^2 \quad (25)$$

and a drag force:

$$F_D = \frac{1}{2} C_D \rho_w D_o (u\cos\alpha + V\cos\beta)\,|u\cos\alpha + V\cos\beta| \quad (26)$$

are imposed based on the Morison's equations [25], where C_L and C_D are the lift and drag coefficients respectively. On top of that, the wave induced acceleration a gives rise to an inertia force:

$$F_I = C_I \rho_w \frac{\pi D_o^2}{4} a\cos\alpha \quad (27)$$

with C_I the inertia coefficient. For combined wave and current action, the hydrodynamic coefficients $\{C_L, C_D, C_I\}$ can be selected [26] based on the surface roughness on the pipe, the Reynolds number *Re*, the Keulegan-Carpenter number K, and the gap between the pipe and the seabed [27]. Current and wave velocity and incidence angle can be supplied directly by the user. The wave parameters can also be calculated based on the JONSWAP spectrum [28]. In this modification of the Pierson-Moskowitz spectrum [29] for a developing sea state in a fetch-limited situation, the significant flow velocity amplitude and the mean zero-up crossing period are calculated based on linear Airy wave theory [30].

Finally, the pipeline loading history, which is fundamental for the realistic simulation of its response, is tracked by defining successive load cases. Loading sequences such as shut-down cycles, can be modelled using restart capabilities, which allows a load case to start from the final configuration of a previous condition.

All of the load patterns described above are converted to nodal forces. The forces acting upon each node are summed, resulting in an out-of-balance force $F(t)$. According to Newton's law, this force implies an acceleration:

$$a(t) = \frac{F(t)}{m} \quad (28)$$

with m the total mass lumped at this node.

To calculate the position of the pipeline over time, a transient dynamic solver uses an explicit integration method. Indeed, the velocities v are obtained from the acceleration using the central difference integration scheme:

$$v\left(t + \frac{\Delta t}{2}\right) = v\left(t - \frac{\Delta t}{2}\right) + \Delta t \cdot a(t) \quad (29)$$

and a similar scheme is used to update the nodal positions p:

$$p(t + \Delta t) = p(t) + \Delta t \cdot v\left(t + \frac{\Delta t}{2}\right) \quad (30)$$

A similar scheme applies for the rotational degrees of freedom. The explicit integration algorithm is conditionally

stable [30], provided the time increment Δt is sufficiently small. For the (dominant) axial deformation mode, critical time step is closely connected to the acoustic velocity, and:

$$\Delta t < L_0 \sqrt{\frac{\rho_s}{E}} \left(\sqrt{1+\xi^2} - \xi \right) \tag{31}$$

must be satisfied to avoid that information propagates over more than one element during one time increment. In (31), ρ_s is the density of steel, and ξ is a damping factor. While an explicit solver offers the potential for dynamic loading and realistic pipelay simulation, the condition in Equn 31 indicates that the initial element length and the time increment must be judiciously chosen to obtain convergence.

By introducing the concept of damping, the explicit (and hence inherently dynamic) approach can also be used to obtain solutions to (quasi-)static problems. Quasi-static load cases are phased in over a period of time, called the ramping time. Once the ramping time is reached, the load reaches its full extent, and the pipe is given time to settle down and reach equilibrium. This quasi-static load introduction is explained on Fig.12.

The total sum of the kinetic energy over all nodes:

$$E_{kin} = \sum_{i=1}^{N} \frac{m_i}{2} v_i^2(t) \tag{32}$$

is a scalar value that indicates the energy content of the entire pipeline as a function of time. As shown in Fig.12, the simulation is assumed to have reached equilibrium when the kinetic energy drops below a pre-defined threshold value E_{th}, or when the equilibrium time is reached.

Numerical prediction of lateral buckling

Pipelines operating at high temperature are susceptible to global buckling. The basics of buckling were first developed by Euler [32], who established the critical load for long, slender, structures under compression. In pipeline engineering, Hobbs [33-34] was one of the first to develop a semi-empirical method to calculate buckling. His approach was based on solving the linear differential equation for the deflected shape of a spring-supported beam-column under axial load. The most important limitations of this method are the assumptions on linear-elastic material and small rotations, and the idealized straight pipeline.

It is recognized [35] that lateral-buckling modes tend to occur at lower compressive forces than the vertical (upheaval) buckling mode. Hence, unless horizontal displacements are restrained (like for buried pipelines) or a prevailing vertical imperfection is present, pipelines tend to buckle laterally. It has even been argued to use lateral buckling as a design tool [36-37] to relieve and control axial compression in the pipeline.

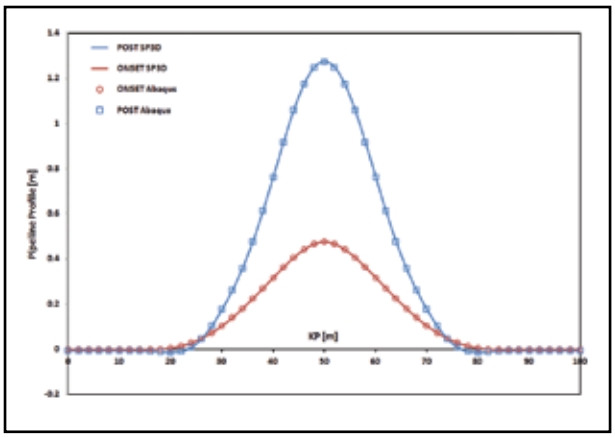

Fig. 14. SAGE Profile upheaval buckling simulation.

In Fig.13, the plan view of an operational pipeline is shown when subjected to increasing temperatures. The simulation has been performed with *SAGE Profile*, using the vertical soil spring for medium dense sand (shown in Fig.9), and lateral and axial friction factors equal to μ = 0.7.

The pipeline path deviates from its original route, and a lateral buckle develops. In post-buckling behaviour, the effective axial force in the buckle zone (which reached the critical value to trigger instability) drops because of the additional length that feeds into the buckle. Simulations have shown [37] that the length of the buckle, its maximum amplitude, and the effective axial force mainly depend on the mechanical material properties, the pipeline geometry and weight, and the pipe-soil interaction.

Susceptibility to upheaval buckling

Buried pipelines subjected to a large temperature increase and axial restraint are prone to upheaval buckling. As a benchmark, a straight 100-m long pipeline, pinned at both ends, was simulated on a rigid frictionless soil. An initial imperfection was introduced at mid-length to invoke upheaval buckling. The *SAGE Profile* simulation results, shown in Fig.14, show excellent agreement with the Abaqus simulations for both the onset of buckling and the post-buckling behaviour.

In addition to these predictive capabilities, the software offers tools to prevent or mitigate the problems associated with upheaval buckling. For instance, the tendency of a buried pipe to lift is decreased by the weight of the backfill soil and the shear resistance generated along the potential failure surface in the backfill soil. This backfill behaviour can be accounted for by including the submerged weight of the soil cover, and incorporating the equivalent shear resistance of the backfill using the Schaminee model [38]:

$$F_c = \gamma_s D_o Z \left(1 + \lambda \frac{Z}{D_o} \right) \tag{33}$$

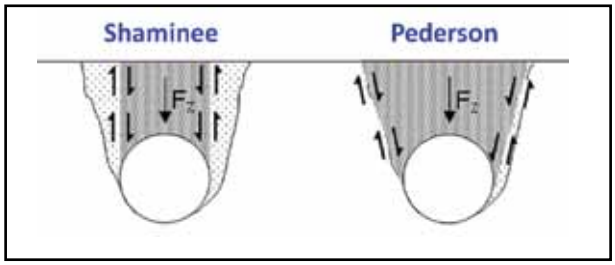

Fig.15. Backfill according to Schaminee and Pederson.

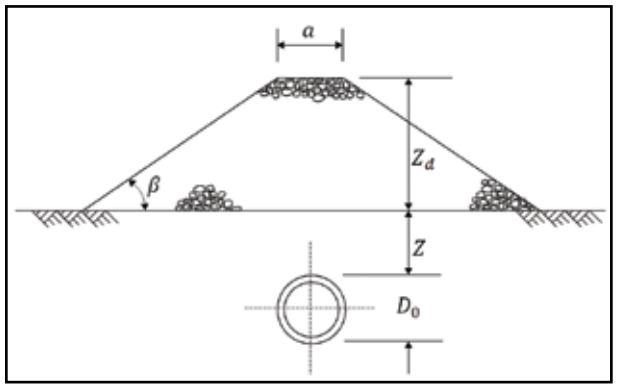

Fig.16. Required volume of rock dump.

or the Pederson formula [39]:

$$F_c = \gamma_s D_o Z \left[1 + 0.1\left(\frac{D_0}{Z}\right) + \lambda\left(\frac{Z}{D_o}\right)\left(1 + \frac{D_o}{2Z}\right)^2\right] \quad (34)$$

where Z is the cover depth (counted from the top of the pipe) and λ is an uplift coefficient, accounting for shear strength. The subtle difference between the soil failure surfaces assumed by Schaminee and Pederson is explained in Fig.15.

In addition to predicting the susceptibility to upheaval buckling, finite-element software can be used as a design tool to optimize the required volume of rock dump to avoid buckling. The design envelope approach described by Richards [40] gives an estimation of the required download:

$$W = \frac{h}{l^2} F_e \left(a + \frac{b}{\psi^2}\right) \quad (35)$$

where a and b are constants, h is the amplitude of the imperfection, l the corresponding imperfection wavelength, and:

$$\psi = l\sqrt{\frac{F_e}{EI}} \quad (36)$$

For a buried pipe, the rock dump should then exert a download equal to:

$$w_d = W - w_p - w_c \quad (37)$$

with w_p and w_c the submerged weight of the pipe and the backfill cover respectively.

The download wd can then be converted to the rock dump volume V_d shown on Fig.16:

$$V_d = a(Z_d + D_0) + \frac{(Z_d + D_0)^2}{\tan\beta} \quad (38)$$

with a the crest width, β the slope angle and Z_d the required rock dump cover depth above the pipe. Note that this approach remains valid for a pipeline sitting on the seabed, with:

$$Z = 0 = w_c \quad (39)$$

Numerical tools can be used to evaluate the influence of seabed modifications, such as the installation of sleepers to promote buckling, rectifying a rough seabed, or finite-element simulation of trenching operations. The post-trench soil behaviour can be reflected by intelligent backfill soil springs as shown in Fig.17, which account for the combined effects of pipe mobilization, cover download, and backfill shear resistance. Such tools allow optimizing rock dumping and controlling the costs associated with seabed interventions.

Pipeline walking simulation

Observations and analysis [41] have shown that short subsea flowlines operating at high temperatures can exhibit pipeline walking [42] and axial creeping [43]. A recent, comprehensive overview on pipeline walking is presented in [44]. Here, *SAGE Profile* is used to demonstrate the importance of pipe soil interaction (and in particular seabed friction) on the likelihood of pipeline walking.

As explained in [44], pipeline walking can cause cumulative axial displacement of an entire pipeline, which can induce damage at termination units, expansion spools and riser tie-ins. The rate of walking depends not only on the temperature profiles, but also on the magnitude of axial resistance, the mobilization distance and the seabed topography.

The main driving mechanisms for pipeline walking are:

- tension, associated with a steel catenary riser
- global seabed slope along the pipeline length
- thermal transients during start-up and shut-down

Although the origin may be different, the walking mechanism for each of these three cases is governed by the effective axial force profile of the pipeline. For a fully restrained, closed-ended pipeline, the effective axial force F_e is the sum of the forces due to axial elongation, internal and external pressure (including end effects), and the temperature gradient ΔT:

$$F_e = \frac{L - L_0}{L_0} EA + (1 - 2\nu)(p_e A_e - p_i A_i) - EA\,\alpha\Delta T \quad (40)$$

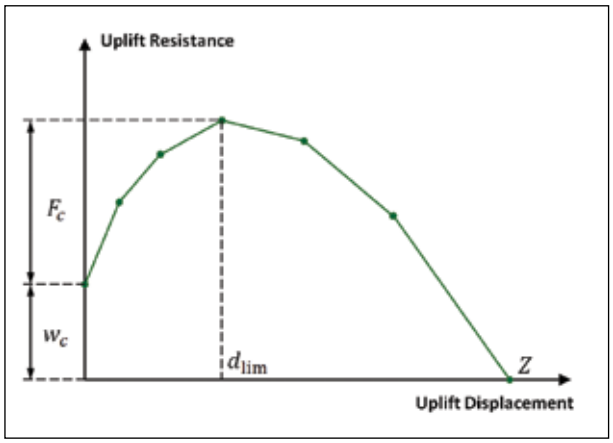

Fig. 17. Smart backfill soil springs for buried pipelines.

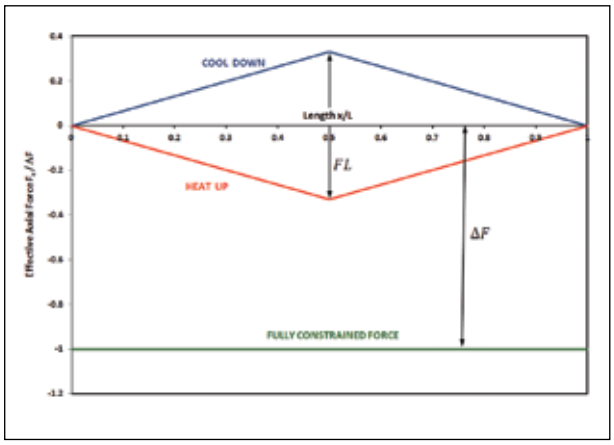

Fig. 18. Force profiles for fully mobilized 'short' pipeline.

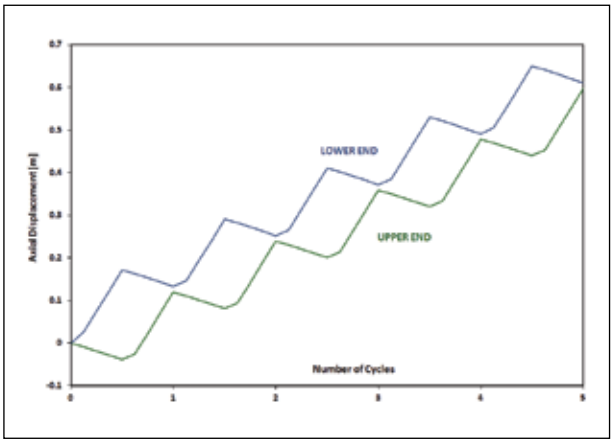

Fig. 19. Pipeline walking over five subsequent cycles.

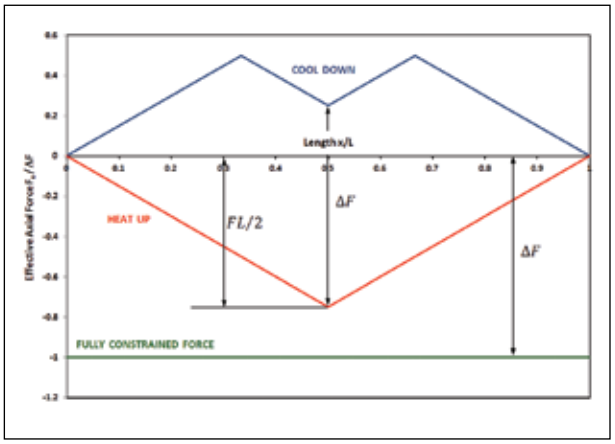

Fig. 20. Force profiles for cyclically constrained pipeline.

with α the coefficient of thermal expansion for steel. During cyclic loading of the pipeline, the change in fully constrained force:

$$\Delta F = -\Delta p\,(1-2\nu)\,A_i - EA\;\alpha\Delta T \tag{41}$$

will dictate the pipeline walking response [44-45]. In this paper, *SAGE Profile* is used to evaluate the influence of seabed friction on the walking rate of a pipeline on an inclined seabed. A straight pipeline of 5000 m length was modelled on an inclined seabed with a slope θ = 15° and subjected a temperature gradient ΔT = 20°. The soft clay, shown in Fig.9, was used as a vertical soil spring. The horizontal soil behaviour was modelled by uncoupled axial and lateral soil springs as shown in Fig.10, i.e. allowing for perfect plasticity and with a memory component; the latter capability is fundamental to accurately model walking, and only the seabed friction μ is varied.

Figure 18 shows the general force profiles in fully heated and cool-down conditions for a 'short' pipeline, i.e. the force envelope does not exceed the fully constrained force ΔF. In this situation, the pipeline is fully mobilized and can freely expand and contract around a virtual anchor point.

Generally, the slope of the force profile is defined by the axial friction $f = \mu\, w_p$. On an inclined seabed, the pipe weight promotes expansion in downhill direction, but counteracts the uphill expansion. This is similar to modifying the friction coefficient:

$$\mu_\theta = w_p(\mu\cos\theta \;\pm\; \sin\theta) \tag{42}$$

which causes an asymmetric force profile envelope [44]. This situation gives rise to a rigid body displacement: the pipe starts to walk down-hill. Figure 19 clearly demonstrates that both pipeline ends move the same amount at the end of each cycle. The walking rate $\Delta\theta$ can be approximated by [44]:

$$\Delta_\theta = \frac{\left(\Delta F + w_p L|\sin\theta| - w_p L\,\mu\,\cos\theta\right) L\tan\theta}{E\,A\,\mu} \tag{43}$$

When the friction factor (or the pipeline length) is increased, the fully constrained force is still sufficient to overcome friction on first load, but not enough to mobilize the pipe during cool-down, as schematically shown in Fig.20. Indeed, the axial friction during cool-down is enough for a certain section of the pipeline to reach fully constrained conditions.

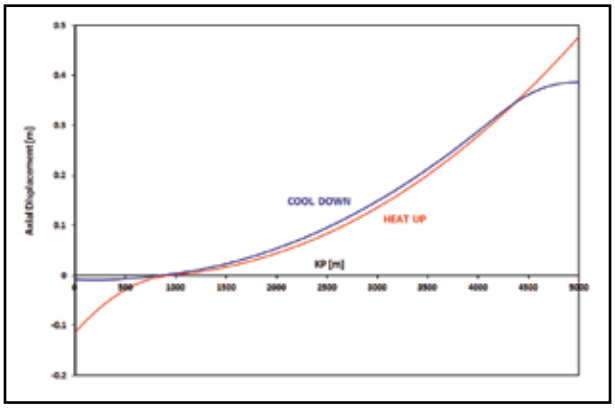

Fig.21. Axial displacement for partially constrained pipe.

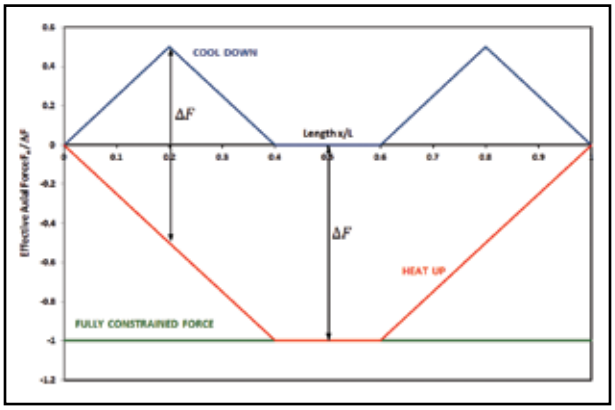

Fig.22. Force profiles for fully constrained pipelines.

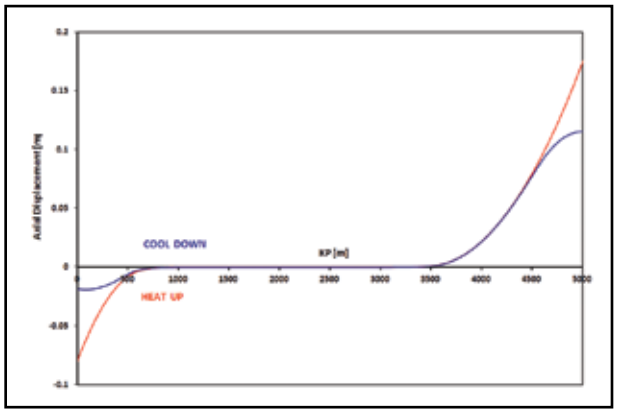

Fig.23. Axial displacement for fully constrained pipe.

Over this length, the pipeline remains anchored and hence cannot move during cool-down. Moreover, since the virtual anchor point of the heat-up stage is located within the anchored length of the cool-down cycle, the pipeline becomes anchored at that location, which prevents walking. The axial displacement during heat-up and subsequent cool-down, predicted by the software, is shown in Fig.21.

When increasing the friction until:

$$\mu_\theta > \frac{2\,\Delta F}{w_p\,L} \tag{44}$$

the pipeline becomes fully constrained. As shown in Fig.22, the pipeline is anchored over a certain length during both cool-down and heat-up. Since the anchored lengths during both phases overlap, the pipeline cannot walk. This is clearly demonstrated by the vanishing axial displacements, shown in Fig.23.

Thanks to the plastic soil springs with memory component (Fig.10), modelling pipeline walking is feasible with *SAGE Profile*. The results for pipeline walking on an inclined seabed, presented here, are in excellent agreement with the theory [44, 45].

Conclusions

In this paper, recent developments in numerical modelling and analysis of offshore pipelines were reviewed and discussed. Finite-element techniques to assist in pipeline design were introduced, and the *SAGE Profile* software suite for offshore pipeline analysis was used to evaluate free-spanning pipelines, simulate lateral and upheaval buckling, and address pipeline walking. The main conclusions from these case studies are:

- Simulation of the pipelaying process is one of the most challenging tasks. An incremental solution was presented, where new elements are fed-in from an anchor point close to the seabed. This elegant approach allows simulating the actual installation process from a laybarge in an efficient fashion, and enables a quick and straightforward assessment of the on-bottom roughness.

- Finite-element simulations of pipelaying can contribute to route optimization, and the assessment of free-spanning pipelines can save a significant amount of time and money associated with seabed rectification.

- The key to a successful simulation of offshore pipeline installation and operation, is a profound understanding of pipe-soil interaction. The pipeline steel can be modelled by a Ramberg-Osgood material model, whereas the soil response is captured by a combination of vertical, axial, and lateral springs. The correct calibration of the pipe-soil interaction parameters is of paramount importance to reach reliable solutions.

- Transient dynamic solvers are based on an explicit integration algorithm. The central differences' scheme is conditionally stable, provided the time increment is sufficiently small. By introducing the concept of damping, the explicit (dynamic) approach can also be used to obtain quasi-static equilibrium.

- *SAGE Profile* can predict the occurrence of lateral and upheaval buckling. In addition to these predictive

capabilities, the software offers tools to prevent or mitigate the problems associated with buckling. Smart backfill soil springs can account for the combined effects of pipe mobilization, cover download, and backfill shear resistance, and calculation of the required download to prevent upheaval buckling contributes to rock-dump optimization.

- Pipeline walking due to seabed slope has been modelled, and the results show excellent agreement with the theory: migration only occurs when the effective axial forces along the entire pipeline remain below the fully restrained conditions during both heat-up and cool-down. Again, the influence of seabed friction on the simulation results was stressed.

- Finite-element tools, such as that described in this paper, provide added value as a design aid and a decision tool throughout the entire life of an offshore pipeline, covering (among other aspects) preliminary design, route optimization, pipelaying, span assessment, and on-bottom stress analysis.

References

1. J.F.Witgens, H.Falepin, and L.Stephan, 2006. New generation pipeline analysis software. Offshore Pipeline Technology Conf.
2. Fugro GeoConsulting, 2010. *SAGE Profile* 3D pipeline analysis software. Technical Brochure.
3. http://www.sage-profile.com (accessed 2012).
4. A.C.Palmer and R.A.King, 2004. Subsea pipeline engineering. PennWell Books.
5. R.Denis and I.Nash, 2012. Desk-top study: the un-exploited resource. *World Pipelines*.
6. Y.Bai and Q.Bai, 2005. Pipelines and risers, Chapter 34: Installation design, pp 597-636.
7. H.S.Choi, 2001. Free spanning analysis of offshore pipelines. *Ocean Engineering*, **28**, pp1325-1338.
8. O.Fyrileiv, 2010. Effect of internal pressure on free spanning pipelines. 8th Int. Pipeline Conference, IPC2010-3162.
9. Det Norske Veritas, 2006. Recommended Practice DNV-RP-F105, Free spanning pipelines.
10. R.E.Hobbs, 1986. Influence of structural boundary conditions on pipeline free span dynamics. International Conference on Offshore Mechanics and Arctic Engineering, OMAE.
11. W.Ramberg and W.R.Osgood, 1943. Description of stress strain curves by three parameters. National Advisory Committee for Aeronautics, Technical note no. 902.
12. W.F.Chen and D.J.Han, 1985. Tubular members in offshore structures, Chapter 2: Moment-curvature relations, pp 21-30.
13. C.E.Murphey and C.G.Langer, 1985. Ultimate pipe strength under bending, collapse and fatigue. Proc. 4th International Conference on Offshore Mechanics and Arctic Engineering, OMAE, pp467-477.
14. S.Gellin, 1980. Plastic buckling of long cylindrical shells under pure bending. *Int.J. Solids and Structures*, **16**, pp397-407.
15. H.Soren and Y.Bai, 1999. Bending moment capacity of pipes. Proc. International Conference on Offshore Mechanics and Arctic Engineering, OMAE.
16. P.E.Winter, J.W.B.Stark, and J.Witteveen, 1985. Collapse behaviour of submarine pipelines. Shell structures, Chapter 7, pp221-226.
17. Det Norske Veritas, 1992. Foundations: Class Notes DNV CN30.4.
18. R.Verley and K.M.Lund, 1995. A soil resistance model for pipelines placed on clay soils. Proc. International Conference on Offshore Mechanics and Arctic Engineering, pp.225-232.
19. J.C.Ballard, H.Falepin, and J.F.Wintgens, 2009. Towards more advanced pipe soil interaction models in finite element pipeline analysis. Proc. Annual Conf. of the Society for Underwater Technology, Perth, Australia.
20. J.Zhang, D.P.Stewart, and M.R.Randolph, 1999. An elasto-plastic model for pipe soil interaction of unburied pipelines in calcareous sands. Proc. International Symposium on Offshore and Polar Engineering ISOPE, pp185-192.
21. Idem, 2002. Modelling of shallowly embedded offshore pipelines in calcareous sand. *J.Geotechnical and Geo-Environmental Engineering*, **128**, 5, pp363-371.
22. R.Denis and C.De Brier, 2010. Deep water tool for soil pipe interaction measurement: recent development and system improvement. Proc. Offshore Technology Conference, OTC-20630.
23. R.A.Jewell and J.C.Ballard, 2011. Axial pipe soil interaction: a suggested framework. Proc. Offshore Technology Conference, OTC-22010.
24. D.J.White, S.A.Ganesan, M.D.Botton, D.A.S.Bruton, J.C.Ballard, and T.Langford, 2011. Observations on axial pipe soil interaction from testing on soft natural clays. Ibid.
25. J.R.Morison, M.P.O'Brien, J.W.Johnson, and S.A.Schaaf, 1950. The forces exerted by surface waves on piles. *J.Petroleum Technology*, **189**, pp149-154.
26. Det Norske Veritas, 2010. Recommended Practice DNV-RP-C205, Environmental conditions and environmental loads.
27. F.Van den Abeele and J.Vande Voorde, 2006. Stability of offshore pipelines in close proximity to the seabed. Proc. 6th Pipeline Technology Conference, Hannover, Germany.
28. R.M.Isherwood, 1987. A revised parameterisation of the JONSWAP spectrum. *Applied Ocean Research*, **9**, 1, pp47-50.
29. Pierson and Moskowitz, 1964. A proposed spectral form for fully developed wind seas based on similarity theory of S.A. Kitaigorodskii. *J.Geophysical Research*, **69**, pp5181-5190
30. T.Sarpkaya and M.Isaacson, 1981. Mechanics of wave forces on offshore structures. Van Nostrand Reinhold, New York.

31. K.J.Bathe, 1996. Finite element procedures. Prentice-Hall Inc.
32. S.P.Timoshenko and J.M.Gere, 1961. Theory of elastic stability, 2nd Edn, McGraw-Hill.
33. R.E.Hobbs, 1981. Pipeline buckling caused by axial loads. *J.Constructional Steel Research*, **1**, 2.
34. R.E.Hobbs and F.Liang, 1989. Thermal buckling of pipelines close to restraints. Proc. International Conference on Offshore Mechanics and Arctic Engineering, OMAE.
35. M.Carr, D.Bruton, and D.Leslie, 2003. Lateral buckling and pipeline walking: a challenge for hot pipelines. Proc. Offshore Pipeline Technology Conference OPT.
36. D.Bruton, M.Carr, M.Crawford, and E.Poiate, 2005. Safe design of hot on-bottom pipelines with lateral buckling using the guideline developed by the SAFEBUCK JIP. Proc. Deep Offshore Technology Conference.
37. D.Kaye, D.LeMarchand, P.Blondin, and M.Carr, 1995. Lateral buckling design of the Dunbar-North Alwyn double wall insulated pipeline. Offshore Pipeline Technology Conference.
38. P.E.L.Schaminee, N.F.Zorn, and G.J.M.Schotman, 1990. Soil response for pipeline upheaval buckling analyses: full scale laboratory tests and modelling. Proc. Offshore Technology Conference, OTC-6486, pp563-572.
39. P.T.Pederson and J.Michelsen, 1988. Large deflection upheaval buckling of marine pipelines. Proc. Symposium on the Behaviour of Offshore Structures, pp965-980.
40. D.M.Richards, 1990. The effect of imperfection shape on upheaval buckling behaviour. *In:* Advances on subsea pipeline engineering and technology, Ed. Ellinas, pp51-66.
41. I.Konuk, 1998. Expansion of pipelines under cyclic operational conditions. Proc. International Conference on Offshore Mechanics and Arctic Engineering, OMAE.
42. D.Perinet and I.Frazer, 2005. Movements of deep water flowlines as a result of pressure and temperature loads and the influence of steel catenary risers. Deep Offshore Technology Conference.
43. K.Tornes, J.Jury, B.A.Ose, and P.Thomson, 2000. Axial creeping of high temperatures flowlines caused by soil racheting. Proc. International Conference on Offshore Mechanics and Arctic Engineering, OMAE.
44. M.Carr, F.Sinclair, and D.Bruton, 2006. Pipeline walking: understanding the field layout challenges and analytical solutions developed for the SAFEBUCK JIP. Proc. Offshore Technology Conference, OTC-17945.
45. C.S.Gaillard and K.Williams, 2005. Pipeline walking. Proc. Offshore Pipeline Technology Conference.